



Published in final edited form as:

Structure. 2010 January 13; 18(1): 73–82. doi:10.1016/j.str.2009.10.015.

## Solution Structure of a Unique G-quadruplex Scaffold Adopted by a Guanosine-rich Human Intronic Sequence

Vitaly Kuryavyi and Dinshaw J. Patel\*

Structural Biology Program Memorial Sloan-Kettering Cancer Center New York, NY, 10065

### Abstract

We report on the solution structure of an unprecedented intramolecular G-quadruplex formed by the guanosine-rich human *chl1* intronic d(G<sub>3</sub>-N-G<sub>4</sub>-N<sub>2</sub>-G<sub>4</sub>-N-G<sub>3</sub>-N) 19-mer sequence in K<sup>+</sup>-containing solution. This G-quadruplex, composed of three stacked G-tetrads containing four *syn* guanines, represents a new folding topology with two unique conformational features. The first guanosine is positioned within the central G-tetrad, in contrast to all previous structures of unimolecular G-quadruplexes, where the first guanosine is part of an outermost G-tetrad. In addition, a V-shaped loop, spanning three G-tetrad planes, contains no bridging nucleotides. The G-quadruplex scaffold is stabilized by a T•G•A triple stacked over the G-tetrad at one end and an unpaired guanosine stacked over the G-tetrad at the other end. Finally, the *chl1* intronic DNA G-quadruplex scaffold contains a guanosine base intercalated between an extended G-G step, a feature observed in common with the catalytic site of group I introns. This unique structural scaffold provides a highly specific platform for the future design of ligands specifically targeted to intronic G-quadruplex platforms.

### Introduction

The diversity of possible G-quadruplex folds adopted by single-stranded guanosine-rich sequences containing four tracts of consecutive guanosine residues interspersed by loop sequences is currently under intensive investigation (reviewed in Davis, 2002; Burge et al., 2006; Phan et al., 2006; Patel et al., 2007; Neidle, 2009; Balasubramanian & Neidle, 2009; Lipps & Rhodes, 2009). We were interested in addressing the solution structure of a consensus motif for DNA promoter sequences found in proto-oncogenes (reviewed in Qin & Hurley, 2008), composed of four successive G<sub>3</sub> guanosine-tracts (in bold),

**G-G-G-N-G-G-G-N-N-N-N-G-G-G-N-G-G-G**

with the aim of probing for new G-quadruplex folds. During sequence design within the framework of this concept, we obtained a well-resolved imino proton NMR spectrum for the 19-mer sequence with a central A-A segment, that contains successive G<sub>3</sub>, G<sub>4</sub>, G<sub>4</sub> and G<sub>3</sub> guanine-tracts as outlined below,

© 2011 Published by Elsevier Inc.

\*Corresponding author: Dinshaw J. Patel Phone: 212-639-7207 FAX: 212-717-3066 pateld@mskcc.org.

**Author Contributions:** VK identified the potential of the *chl1* intronic DNA sequence for G-quadruplex formation, as well as recorded and interpreted the NMR spectra and undertook the computations leading to structure determination under the guidance of DJP. VK noted the similarities with group I intronic sequences and formulated the proposed model for phosphoryl transfer at a quadruplex-duplex junction. DJP and VK jointly wrote the paper.

**Publisher's Disclaimer:** This is a PDF file of an unedited manuscript that has been accepted for publication. As a service to our customers we are providing this early version of the manuscript. The manuscript will undergo copyediting, typesetting, and review of the resulting proof before it is published in its final citable form. Please note that during the production process errors may be discovered which could affect the content, and all legal disclaimers that apply to the journal pertain.

**G1-G2-G3-T4-G5-G6-G7-G8-A9-A10-G11-G12-G13-G14-T15-G16-G17-G18-T19**

This sequence (Figure 1A) exhibited imino proton NMR characteristics of a single conformation in  $K^+$ -containing solution, amenable for structural characterization (Figure 1B). A search for the corresponding sequence pattern in the human genome revealed its presence in the 5'-intron of the human *chl1* gene with the exact sequence spanning positions 214.844 to 214.863 on chromosome 3 (Kent et al., 2002) shown below

**C-G-G-G-C-G-G-G-A-A-G-G-G-T-G-G-G-A**

This observation is relevant considering the recent insight from bioinformatics searches of conserved guanosine-rich tracts with the potential to form polymorphic G-quadruplex folds in the first intron of human genes (Eddy & Maizels, 2008, 2009).

In addition, the *CHL1* gene product belongs to the family of FANCI helicases, a group of DNA dependent ATPases capable of catalytically resolving G-quadruplex-forming blocks generated at guanosine-rich tracts, that can impede DNA replication (Wu et al., 2008; 2009).

Here we report on the solution structure of the *chl1* intronic G-quadruplex in  $K^+$ -containing aqueous solution and demonstrate that it adopts an unprecedented G-quadruplex fold exhibiting two unanticipated conformational features, one of which has not been observed previously in the unimolecular G-quadruplex topology literature (reviewed in Burge et al., 2006; Patel et al., 2007).

Surprisingly, the G-quadruplex solution structure of this guanosine-rich consensus sequence identified for a particular intron in the human genome exhibits certain features in common with the catalytic site of group I introns.

## Results

### NMR Spectra and Spectral Assignments

The imino proton NMR spectrum of the *chl1* intronic sequence in 50 mM  $K^+$ -containing  $H_2O$  buffer solution at 25 °C is characterized by twelve well-resolved resonances in the 11–12 ppm range (Figure 1B), a spectral region consistent with guanosine imino N-H protons hydrogen bonded to nitrogen acceptors (N-H••N), as observed for G-tetrads involved in G-quadruplex formation

We pursued a strategy of initially assigning the guanosine imino protons by incorporating 2%  $^{15}N$ -labeled-guanosines one at a time into the oligonucleotide sequence (Figure 1C) and then correlating these unambiguous assignments with guanosine H8 protons (Figure 1D), through long-range through-bond J-coupling experiments (Figure 1E) (Phan, 2000; Phan & Patel, 2002). The resulting guanosine imino proton assignments of the *chl1* intronic sequence are listed above the control NMR spectrum in Figure 1B, and are analyzed in the context of the four-guanosine tracks G1-G2-G3, G5-G6-G7-G8, G11-G12-G13-G14 and G16-G17-G18 within the 19-mer sequence (Figure 1A). We anticipated that three guanosines within each track would be involved in G-quadruplex formation. Nevertheless, the imino proton of G3 at 10.55 ppm, which originates in the first G1-G2-G3 tract, is both broad and resonates upfield of the 11 to 12 ppm region (Figure 1b), suggestive of a guanosine imino proton not involved in N-H••N hydrogen bond formation. In addition the imino proton of G8, though narrow, resonates upfield at 9.95 ppm, indicative of a guanosine imino proton hydrogen-bonded to oxygen acceptors (N-H••O). These results are consistent with involvement of G1-G2, G5-G6-G7, G11-G12-G13-G14 and G16-G17-G18 guanosine-tracts in G-quadruplex formation. Thus, rather than an expected  $G_3-G_3-G_3-G_3$  alignment of

guanosine-tracts required to form a standard G-quadruplex, the *chl1* intronic sequence adopts an unanticipated G<sub>2</sub>-G<sub>3</sub>-G<sub>4</sub>-G<sub>3</sub> alignment of guanosine-tracts.

The remaining non-exchangeable base and sugar protons of the *chl1* intronic sequence were assigned using standard protocols by through-space (NOESY) and through-bond (COSY, TOCSY, <sup>13</sup>C-GHSQC) experiments in 50 mM K<sup>+</sup>-containing <sup>2</sup>H<sub>2</sub>O buffer solution. In case of spectral overlap, resonance assignments were facilitated following 8-bromoguanosine (at positions 1, 5, 11 and 16) for guanosine substitutions, as well as deoxyuridine (at position 15) for thymine substitutions. The expanded NOESY contour plot (200 ms mixing time) in 50 mM K<sup>+</sup>-containing <sup>2</sup>H<sub>2</sub>O buffer at 25 °C correlating base and sugar H1' protons, together with assignment connectivities (base proton to its own and 5'-flanking sugar H1' protons), is shown in Figure 2A. The complete tabulation of base and sugar proton chemical shifts are listed in Table S1 (Supplementary Materials).

The expanded NOESY stacked plot (50 ms mixing time) correlating base with sugar H1' NOEs of the *chl1* intronic sequence in 50 mM K<sup>+</sup>-containing <sup>2</sup>H<sub>2</sub>O buffer at 25 °C exhibits four strong cross peaks for G1, G5, G11 and G16 residues (Figure 2B), indicative of *syn* torsion angles for these four guanosines (short base to sugar H1' distances of 2.5 Å; Patel et al., 1982) in the folded structure of the G-quadruplex in solution. In addition, four guanosine imino protons, assigned to G1, G6, G17 and G13, exchange slowly, as recorded 45 min after transferring (following lyophilization) the *chl1* intronic sequence from 50 mM K<sup>+</sup>-containing H<sub>2</sub>O solution to its <sup>2</sup>H<sub>2</sub>O counterpart at 25 °C (Figure 2C). These results establish that four guanosines G1, G6, G17 and G13 must originate from the central G-tetrad (slowest exchanging guanosine imino protons due to shielding from exchange with solvent) of the G-quadruplex.

### G-tetrad Alignments

We have assigned guanosines to the three G-tetrad planes by monitoring NOEs between guanosine imino and H8 protons between adjacent guanosines around individual G-tetrad planes (Figure 3A) in the NOESY spectrum (mixing time 300 ms) of the *chl1* intronic G-quadruplex in 50 mM K<sup>+</sup>-containing H<sub>2</sub>O solution at 25 °C (Figure 3B). Thus, the imino proton of G1 shows an NOE to the H8 proton of G13 (labeled G1/G13 in orange), the imino proton G13 shows an NOE to the H8 proton of G17, the imino proton of G17 shows an NOE to the H8 proton of G6, and the imino proton of G6 shows an NOE to the H8 proton of G1, thereby assigning the guanosines and their order around the G1•G13•G17•G6 G-tetrad plane (assignments in orange) (Figures 3B–D). Related NOE tracings identify the G7•G11•G14•G18 (assignments in red) and G2•G5•G16•G12 (assignments in blue) G-tetrads that form the G-quadruplex (Figures 3B–D). Since the imino protons of the G1•G13•G17•G6 G-tetrad exhibit the slowest exchange rate (Figure 2C), this central G-tetrad must be bracketed on either side by stacked G7•G11•G14•G18 and G2•G5•G16•G12 G-tetrads, resulting in the backbone tracing from G1 to G18 as shown in Figure 3D.

### G-Quadruplex Folding Topology

The *chl1* intronic G-quadruplex folding topology shown in Figure 3D contains *syn* guanosines at G1, G5, G11 and G16, and *anti* guanosines at the remaining positions, consistent with the short mixing time NOESY data (Figure 2B). Unexpectedly, the first guanosine in the sequence, G1, is positioned within the central G-tetrad of the G-quadruplex. The G1-G2 segment forming the first column spans the lower two G-tetrad planes, and is followed by the G3-T4 segment which forms an edge-wise loop, leading into the G5-G6-G7 segment of the second column that spans all three G-tetrad planes. Next, the G8-A9-A10 segment forms a second edge-wise loop, leading into the G11-G12 step with its extended sugar-phosphate backbone, whereby G11 of the top G-tetrad is directly connected

in a V-shaped extended alignment to G12 of the bottom G-tetrad, located on adjacent columns. The G12-G13-G14 segment that forms the third column, is connected to G16-G17-G18 segment that forms the fourth column of the G-quadruplex, by a single-residue (T15) double chain reversal loop.

### Structure Calculations

Initial distance-restrained and subsequent intensity-restrained molecular dynamics calculations (see Methods section) of the solution structure of the *chl1* intronic G-quadruplex were guided by exchangeable and non-exchangeable proton restraints, with the restraints listed by category in Table 1. The ensemble of 17 refined superpositioned structures is shown in stereo in Fig 4A, with a representative refined structure shown in a ribbon representation in Figure 4B and a surface representation in Figure 4C. The ensemble of refined structures is well converged, exhibiting pair-wise root-mean-square-deviation (rmsd) values in the 0.47 range for all nucleotides except for the T15 residue (Table 1), which is confined to a cluster of energetically preferred conformations pointing outwards from the groove (Figure 3A).

Both the top (G8-A9-A10) and bottom (G3-T4) lateral loops are structured within the *chl1* intronic G-quadruplex fold. The top loop is stabilized by a T19•G8•A10 triple (Figure 5A), which stacks on the top G7•G11•G14•G18 tetrad (Figure 5B), while G3 of the bottom loop stacks on the G2•G5•G16•G12 tetrad (Figure 5C). Finally, A9 is unpaired and stacks on top of the T19•G8•A10 triple (Figure 5D).

### Analysis of Modified Sequences

We have systematically probed specific structural elements within the proposed *chl1* intronic G-quadruplex fold by base substitutions so as to gain insights into the range of tolerated mutations by the adopted scaffold and to derive a consensus sequence for bioinformatics analysis.

As expected from the G-quadruplex topology (Figure 3D), unpaired residue A9 positioned on top of the T19•G8•A10 triple (Figure 5D), can be substituted by G, T or C, with no impact on the imino proton spectrum (Figure S1, Supplementary Materials). Similarly, replacement of unpaired residue T4 by G, T or C, and unpaired residue T15 by C15, has no impact on the imino proton spectrum (Figure S2). It is noteworthy that the G-quadruplex folding topology was retained followed replacement of T4 by G4, despite formation of the resulting G<sub>8</sub> segment, involving eight consecutive guanosines at the 5'-end of the sequence.

By contrast, replacement of unpaired residue G3 by I, T and A resulted in doubling of imino proton spectra (Figure S3), indicative of a role for the 2-amino protons of G3 in stabilizing the G3-T4 edge-wise loop of the G-quadruplex fold. Replacement of the 3'-terminal residue T19, which is involved T19•G8•A10 triple formation, by C, A and G, results in progressive deterioration of imino proton spectral quality, despite retaining the overall spectral pattern (Figure S4), consistent with T19 contributing to the stabilization of the G8-A9-A10 edge-wise loop of the G-quadruplex fold, as a consequence of hydrogen bonding to G8 of the sheared G•A non-canonical pair (Figure 5A). As a result of the mutation studies, the consensus sequence compatible with the fold reported here is **G<sub>3</sub>NG<sub>4</sub>NAG<sub>3</sub>(A/C/T)G<sub>3</sub>(A/C/T)** and might provide useful constraints in future bioinformatics searches for intronic G-quadruplex folds.

## Discussion

The recent demonstration of guanosine-rich repeats with the potential for formation of polymorphic G-quadruplex scaffolds within the first intron of human genes (Eddy & Maizels, 2008, 2009), has highlighted the need to elucidate the diversity of G-quadruplex folding topologies adopted by human intronic guanosine-rich repeats.

To this end, we have solved the solution structure of an unique intramolecular G-quadruplex formed by the *chl1* human intronic sequence in K<sup>+</sup> solution. Inspection of the sequence

**G1-G2-G3-T4-G5-G6-G7-G8-A9-A10-G11-G12-G13-G14-T15-G16-G17-G18-T19**

shows that four guanosine-rich tracts are separated by a single (T4), double (A9-A10) and single (T15) connecting segments, suggesting the potential for formation of an all-parallel-stranded G-quadruplex involving three stacked G-tetrads connected by double-chain-reversal loops, as reported for the four guanosine-rich *c-myc* (Phan et al., 2004; Ambrus et al., 2005) and *c-kit1* (Phan et al., 2007) sequences. However, this is not the case since we observe a new G-quadruplex folding topology containing two unanticipated conformational features, one of which has not been reported previously for unimolecular G-quadruplexes.

### First Guanosine is Positioned within the Central G-tetrad

The first striking feature is that the first guanosine G1 is part of the central G-tetrad (Figure 3D), in contrast to the first guanosine having always been reported to be part of a terminal G-tetrad in all unimolecular G-quadruplexes reported to date (reviewed in Patel et al., 2007; Neidle, 2009) Thus G11 and the G1-G2 step that are part of the same column are not connected to each other, in contrast to the unbroken linkage for the three other G5-G6-G7, G12-G13-G14 and G16-G17-G18 columns of the *chl1* intronic G-quadruplex (Figure 3D). It should be noted that an earlier report did identify a bimolecular G-quadruplex where the first guanosine was also part of a central G-tetrad for one of the strands (Crnugelj et al., 2003).

### A V-shaped Loop Spanning Three G-tetrad Planes

Our group first identified the V-shaped loop topology for G-quadruplex folds (Zhang et al., 2001), where guanosines at adjacent corners of stacked G-tetrads are directly connected, resulting in a missing support column. The first example of a V-shaped loop within a G-quadruplex scaffold linked two adjacent G-tetrads as shown in Figure 3E (Zhang et al., 2001), with later examples identified for dimeric G-quadruplexes formed by d(G<sub>3</sub>T<sub>4</sub>G<sub>4</sub>) (Crnugelj et al., 2003) and d(GLGLT<sub>4</sub>GLGL), where L is a locked nucleic acid (Nielsen et al., 2009), contained V-shaped loops that spanned three G-tetrad planes as shown in Figure 3F. The V-shaped loop motif represented in Figure 3F is observed for the unimolecular *chl1* intronic G-quadruplex (Figure 3D), where G11 belongs to the top G-tetrad of one column while G12 belongs to the bottom G-tetrad of an adjacent column, accompanied by an extension of the backbone at the G11-G12 step. In essence, a second striking feature is that the G1 base is partially intercalated between two guanosine bases G11 and G12 within the folding topology of the *chl1* intronic G-quadruplex (Figure 4B).

### Stacked T19•G8•A10 Triple Stabilizes Edge-wise G8-A9-A10 Loop

The T19•G8•A10 triple involves a sheared G8•A10 pair alignment involving pairing of the minor groove edge of G8 with the major groove edge of A10 (Figure 5A), as reflected in the NOEs within the sheared pair and with the stacked adjacent G7•G11•G14•G18 tetrad. The O4 carbonyl group of T19 is hydrogen-bonded to the imino proton of G8 in the T19•G8•A10 triple, readily explaining the upfield shifted 9.95 ppm imino proton chemical shift of G8, characteristic of a guanosine imino proton hydrogen-bonded to an oxygen

acceptor (N-H••O). Replacement of T19 by A and G, but not C, results in deterioration in imino proton spectral quality (Figure S4). The O4 carbonyl is common to both T and C, but not to the purines, emphasizing its importance as an acceptor for the hydrogen bond from the imino proton of G8. In addition, the larger size of the purine ring at position 19 would be more difficult to accommodate as part of a triple on top of the adjacent G7•G11•G14•G18 tetrad.

Consistent with the structure, unpaired A9, which stacks on the T19•G8•A10 triple, can be replaced by G, T and C, without impacting on the imino proton NMR spectrum (Figure S1). Since A9 is well-defined in the structure, the conformation of the connecting sugar-phosphate is more important for the G8-A9-A10 edge-wise loop than the base at position 9.

### Stacked G3 Stabilizes Edge-wise G3-T4 Loop

The two-residue bottom edge-wise loop is composed of residues G3 and T4. They form a configuration where T4 is stacked on top of the G3, which in turn is stacked on the G2•G5•G16•G12 G-tetrad (Figure 5C). We observe a single average resonance for the two amino protons of G3, in contrast to separate hydrogen-bonded and exposed amino protons for guanines involved in G-tetrad formation. The average amino protons of G3 exhibit cross-peaks to the imino protons of all four guanines in the G2•G5•G16•G12 G-tetrad (peaks j, k, l, m in Figure 3B), consistent with the overlap geometry shown in Figure 5C, where the G3 amino protons are stacked over the center of the adjacent G-tetrad.

Replacement of G3 by I3, T3 or A3, results in doubling of the imino proton NMR spectra, including the upfield shifted imino proton of G8 at 9.95 ppm (Figure S3), indicative of an equilibrium between two G-quadruplex folds for the substituted analogs. Guanosine has an amino proton at the 2-position, which is missing in inosine and adenosine. It is conceivable that a K<sup>+</sup> ion may be sandwiched between G3 and the G2•G5•G16•G12 G-tetrad, and that monovalent cation coordination requires the presence of an amino group at the 2-position of the purine ring, to stabilize a single G-quadruplex conformation. The proposed coordinated K<sup>+</sup> cation could also slow down the exchange of the imino proton of G3, thereby accounting for the observation of a broadened resonance at 10.55 ppm (Figure 1B).

### A Double-chain-reversal Loop

The parallel alignments of the G12-G13-G14 and G16-G17-G18 segments are bridged by a single residue (T15) double-chain-reversal loop in the structure of the *chl1* intronic G-quadruplex (Figures 4A and 4B). Such double-chain-reversal loops were first reported a decade and a half ago by our group for the four-guanosine repeat *Tetrahymena* G-quadruplex (Wang & Patel, 1994), but came into greater prominence with their observation in the crystal structures of two- and four-guanosine repeat human telomere G-quadruplexes by the Neidle laboratory (Parkinson et al., 2002). Single residue double-chain-reversal loops spanning three G-tetrad planes, as observed for *chl1* intronic G-quadruplex (Figure 3D), were first reported for the G-quadruplex formed by the four-guanosine repeat segment of the *c-myc* promoter (Phan et al., 2004; Ambrus et al., 2005).

### Recognition properties of *chl1* intronic G-quadruplex

The *chl1* intronic G-quadruplex has a distinct pattern of grooves, which sets it apart from other known G-quadruplexes formed in the vicinity of transcription start sites, such as *ckit* (Phan et al., 2007) and *c-myc* (Phan et al., 2004; Ambrus et al., 2005) promoter G-quadruplexes. The start of the fold in the middle G-tetrad and zero-residue bridging of the G11-G12 step imposes restrictions on the accessibility of the groove formed by the G11-break-G1-G2 and G12-G13-G14 columns (Fig. 4A). The adjacent groove between columns G12-G13-G14 and G16-G17-G18, which is bridged by single residue T15, is accessible for

hydrogen-bond recognition the guanine edges of its G-tetrad and its outwardly-pointed T15 base. The two remaining grooves are completely accessible for hydrogen-bond recognition by small drugs or protein side chains. The two lateral loops positioned above and below the G-quadruplex also have potential for hydrogen bond recognition involving accessible base edges of the G8•A10•T21 base triple (Figure 5A), the single base A9 in the 3'-end loop (Figure 5D), and bases G3 and T4 in the 5'-end loop (Figure 5C). In contrast to *c-kit* and *c-myc* promoter G-quadruplexes, the *chl1* intronic G-quadruplex has only one single-residue double-chain reversal loop and a unique pattern of guanine bases constituting the quadruplex core. The 5'- and 3'-ends of the *chl1* intronic G-quadruplex are positioned on adjacent stacked G-tetrads and positioned diagonally across the G-quadruplex (Figure 3D).

### Comparison with the Active Site of Group I Introns

A novel feature of the solution structure of the *chl1* intronic G-quadruplex is the partial intercalation of G1 between two other guanines, each of which is involved in G-tetrad formation (Figure 6E). We therefore searched data bases for related alignments amongst higher order RNA folds and found a similar arrangement within the G-binding motif in the catalytic core of group I intron ribozymes (Adams et al., 2004; Guo et al., 2004; Golden et al., 2004; reviewed in Stahley & Strobel, 2006). Indeed, in the 3.1 Å crystal structure of *Azoarcus* group I intron in complex with both 5'- and 3'-splice sites, corresponding to the splicing intermediate before the exon ligation step, the terminal nucleotide of the intron, ΩG206, partially intercalates between G128 and A127, as part of an anchored G-binding motif (Adams et al., 2004; Figure 6A). Partial intercalation of ΩG206 between purine bases (Figures 6B and 6C) and its pairing with the Hoogsteen edge of G130 (Figure 6D) in the *Azoarcus* group I intron (Adams et al., 2004) has striking parallels with partial intercalation of G1 between G11 and G12 (Figures 6E and 6F), with G1 paired with the Hoogsteen edge of G13 as part of the G1•G13•G17•G6 G-tetrad (Figure 6G) in the *chl1* intronic G-quadruplex. One difference between these two alignments is that the sugar ring oxygens of ΩG206 in the intron (Figure 6B) and G1 in the G-quadruplex (Figure 6E) are oriented in opposite directions.

### A Proposed Model for Phosphoryl Transfer Mediated by a G-Quadruplex Scaffold

A unique feature of the group I catalytic pocket is the in-line position of the activated 5'-exon 2'-OH and the conformationally constrained scissible phosphate at the intron-3'-exon junction, which is bracketed on either side by Mg<sup>2+</sup> cations (Figure 6A; Stahley & Strobel, 2005). Such alignments, involving a constrained guanosine, define splice site selection during catalyzed phosphoryl transfer between guanosine and a substrate RNA strand (reviewed in Stahley & Strobel, 2006). We propose that the guanosine flanking the scissible phosphate can be equally well locked into position either through partial intercalation (Figures 6B and 6C) and base triple formation (Figure 6D) as observed for ΩG206 in the group I intron (Adams et al., 2004) or through partial intercalation (Figures 6E and 6F) and G-tetrad formation (Figures 6G) as observed for G1 in the *chl1* intronic G-quadruplex.

We therefore propose a model of a higher order RNA structure where a constrained guanosine as part of a G-quadruplex could participate in the splicing reaction at a quadruplex-duplex junction as shown schematically in Figure S5. The RNA duplex is on the left and the RNA G-quadruplex is on the right, with the 5' and 3'-ends of the RNA labeled in Figure S5. A distinction between the experimentally determined group I intron splice site (Figure 6A) and the proposed model of the quadruplex-duplex junctional splice site (Figure S5B; expanded view of Figure S5A) is that the attacking nucleophile is a 3'-OH group in the former structure and a 5'-OH group in the latter model. The model in Figure S5A has been

proposed in the spirit of stimulating further experiments at comprehensive molecular engineering of higher-order G-quadruplex folds and clearly needs experimental validation.

Our structure of the *chlI* intronic G-quadruplex raises the issue as to whether a DNA segment can be accommodated 5' to the first guanosine that is part of the central G-tetrad of the *chlI* intronic DNA G-quadruplex. Our modeling studies shown in Fig. S5A indicate that there is ample room to accommodate such a DNA segment without perturbing this unique G-quadruplex fold.

## Summary and Future Prospects

The G-quadruplex fold adopted by the human *chlI* intronic sequence in K<sup>+</sup>-containing solution, composed of three G-tetrads containing four *syn* guanines, exhibits conformational features not reported previously for unimolecular G-quadruplexes. The unprecedented combination of the first guanosine being part of the central G-tetrad, together with a V-shaped loop spanning three G-tetrad planes without an intervening nucleotide, results in intercalation of the G1 base between an extended G11-G12 step. Strikingly, this intercalation alignment is similar to what has been observed in the catalytic core of group I introns, an alignment that facilitates catalyzed phosphoryl transfer reactions. The novel topology of the *chlI* intronic G-quadruplex makes this scaffold a unique platform for future structure-based ligand design (reviewed in Patel et al., 2007; de Cian et al., 2008; Ou et al., 2008; Monchaud & Teulade-Fichou, 2008; Neidle, 2009; Balasubramanian & Neidle, 2009).

## Methods

### Sample preparation

The unlabeled and the site-specific low-enrichment (2% uniformly-N<sup>15</sup>-labeled) oligonucleotides were synthesized and purified as described previously (Phan, 2000; Phan & Patel, 2002). The strand concentration of the sample was typically in the range 0.5 to 5.0 mM and was dissolved in 50 mM KCl, 5 mM K-phosphate buffer, pH 6.8.

### NMR spectroscopy

Experiments were performed on 600 MHz Varian NMR spectrometers with data recorded at 25 °C. Guanosine base resonances were assigned unambiguously by using site-specific low-enrichment labeling and through-bond correlation at natural abundance (Phan, 2000; Phan & Patel, 2002). Assignment for some residues were verified and confirmed in independently synthesized samples with specific substitutions. Spectral assignments were also assisted and supported by COSY, TOCSY, <sup>13</sup>C-HSQC and NOESY spectra. Interproton distances involving exchangeable protons were categorized as strong (2.8 to 5.2 Å), medium (3.15 to 5.85 Å) or weak (3.5 to 6.5 Å) based on cross-peak intensities recorded in a NOESY spectrum (50 and 300 ms mixing time) in H<sub>2</sub>O solution. Interproton distances involving non-exchangeable protons were measured from NOE build ups using NOESY experiments recorded at five mixing times (50, 100, 150, 200 and 250 ms) in <sup>2</sup>H<sub>2</sub>O solution.

### Structure Calculations

The structures of the *chlI* intronic G-quadruplex were calculated using the X-PLOR program (Brünger, 1992) as described previously (Phan et al., 2007). The initial folds guided by NMR restraints listed in Table 1 were obtained using torsion dynamics. The structures were further refined by Cartesian dynamics and, finally, using relaxation matrix refinement.

The initial structure consisted of an extended DNA strand with randomized chain torsion angles of constituent nucleotides, whose angles and bonds were set up in accordance with most updated measurements (Gelbin et al., 1996; Clowney et al., 1996)



Torsion dynamics: In the heating stage, the regularized extended DNA chain was subjected to 60 ps of torsion-angle molecular dynamics at 40,000 K using a hybrid energy function composed of geometric and NOE terms. The van der Waals (vdW) component of the geometric term was set to 0.1, thus facilitating torsional bond rotations, while the NOE term included NOE-derived distances with the scaling factor of 150. The structures were then slowly cooled from 40,000 K to 1,000 K over period of 60 ps during which the vdW term was linearly increased from 0.1 to 1. At the third stage, the molecules were slowly cooled from 1000 K to 300 K for 6 ps of Cartesian molecular dynamics (Stein et al., 1997). The 35 best structures with no 0.5 Å violations and minimal energies were selected for further refinement.

Distance restrained molecular dynamics: Cartesian molecular dynamics was initiated at 300 K and the temperature was gradually increased to 1000 K during 7 ps. The system was equilibrated for 0.5 ps, while the force constants for the distance restraints were kept at 1 Kcal mol<sup>-1</sup> Å<sup>-2</sup>. Subsequently, the force constants were linearly scaled up to 150 during 17.5 ps. The system was then slowly cooled to 300 K in 14 ps and equilibrated at 300 K for 12 ps. The coordinates saved every 0.5 ps during the last 4.0 ps were averaged. The resulting average structure was subjected to minimization until the gradient of energy was less than 0.1 Kcal mol<sup>-1</sup>. The soft planarity restraints imposed on the G-tetrads with the weight 10 kcal mol<sup>-1</sup> Å<sup>-2</sup> before the heating process, were removed at the beginning of equilibration stage. The electrostatic term was excluded from the energy function to increase the weight of covalent geometry terms during minimization process. The dihedral and hydrogen-bonding restraints for G-tetrad formation were maintained throughout the computations. The 17 best structures were selected at this stage.

Relaxation matrix intensity refinement: To account for spin diffusion effects, all 17 distance refined structures were next subjected to the energy minimization with back-calculation of the NOESY spectra with X-PLOR (Nilges et al., 1991). The relaxation matrix was set up for the non-exchangeable protons, with the exchangeable imino and amino protons replaced by deuterons. NOE intensity volumes from 178 non-exchangeable cross-peaks for each of five mixing times (50, 100, 150, 200, 250) were used as restraints, with uniform upper and lower bounds of ±30%. Dynamics was started at 5 K, and the system was heated up to 300 K in 0.6 psec. During the subsequent relaxation the force constant for NOE intensities was gradually increased from 0 to 300 Kcal mol<sup>-1</sup> Å<sup>-2</sup> with simultaneous decrease of the distance force constant of non-exchangeable protons from 50 to 30 Kcal mol<sup>-1</sup> Å<sup>-2</sup>. The force constant for exchangeable protons and hydrogen bonds was kept at 100 Kcal mol<sup>-1</sup> Å<sup>-2</sup>. After equilibration at 300 K for 3.0 ps the resulting structure was subjected to minimization until the gradient of energy was less than 0.1 Kcal mol<sup>-1</sup>. The NMR R-factor (R<sub>1/6</sub>) improved from initial value of 6.0% to 2.0% with simultaneous improved structure convergency.

### Proposed Model for Phosphoryl Transfer Mediated by a G-Quadruplex Scaffold

The *chlI* intronic RNA G-quadruplex was modeled by rmsd fitting of individual RNA nucleotides onto the DNA G-quadruplex structure (presented here) using common base atoms as superposition targets. All torsion angles of DNA residues except the sugar pucker pseudorotation angle (P) were copied into RNA nucleotides. The junction between the G-quadruplex and duplex was modeled using the *Azoarcus* group I intron junction as a prototype, with inversion of duplex orientation in order to form the connection with the 5'-end G1 of the *chlI* G-quadruplex. The initial model was built manually and subsequently refined by energy minimization using the Discover module of Insight II software.

## Data Deposition

The coordinates for the *chl1* intronic G-quadruplex have been deposited in the Protein Data Bank (accession code: 2KPR).

## Supplementary Material

Refer to Web version on PubMed Central for supplementary material.

## Acknowledgments

The research was supported by NIH Grant GM34504 to D.J.P. He is a member of the New York Structural Biology Center supported by NIH Grant GM66354.

## References

- Adams PL, Stahley MR, Kosek AB, Wang J, Strobel SA. Crystal structure of a self-splicing group I intron with both exons. *Nature*. 2004; 430:45–50. [PubMed: 15175762]
- Ambrus A, Chen D, Dai J, Jones RA, Yang D. Solution structure of the biologically relevant G-quadruplex element in the human *c-MYC* promoter. Implications for G-quadruplex stabilization. *Biochemistry*. 2005; 44:2048–2058. [PubMed: 15697230]
- Balasubramanian S, Neidle S. G-quadruplex nucleic acids as therapeutic targets. *Curr. Opin. Chem. Biol.* 2009; 13:345–353. [PubMed: 19515602]
- Brünger, AT. *A System for X-ray Crystallography and NMR*. Yale University Press; New Haven: 1992. X-PLOR.
- Burge SE, Parkinson GN, Hazel P, Todd AK, Neidle S. Quadruplex DNA: sequence, topology and structure. *Nucleic Acids Res.* 2006; 34:5402–5415. [PubMed: 17012276]
- Clowney L, Jain SC, Srinivasan AR, Westbrook J, Olson WK, Berman HM. Geometric parameters in nucleic acids: nitrogenous bases. *J. Am. Chem. Soc.* 1996; 118:509–518.
- Crnogelj M, Sket P, Plavec J. Small change in a G-rich sequence, a dramatic change in topology: New dimeric G-quadruplex folding motif with unique loop orientations. *J. Am. Chem. Soc.* 2003; 125:7866–7871. [PubMed: 12823005]
- Davis GT. G-Quartets 40 years later: from 5'-GMP to molecular biology and supramolecular chemistry. *Angew. Chem. Int. Edn.* 2004; 43:668–698.
- De Cian A, Lacroix L, Douarre C, Temeime-Smalli N, Trentesaux C, Riou J-F, Mergny J-L. Targeting telomeres and telomerase. *Biochimie*. 2008; 90:131–155. [PubMed: 17822826]
- Eddy J, Maizels N. Conserved elements with potential to form polymorphic G-quadruplexes in the first intron of human genes. *Nucleic Acids Res.* 2008; 36:1321–1333. [PubMed: 18187510]
- Eddy J, Maizels N. Selection for the G4 DNA motif at the 5' end of human genes. *Mol. Carcinog.* 2009; 48:319–325. [PubMed: 19306310]
- Gelbin A, Schneider B, Clowney L, Hsieh S-H, Olson WK, Berman HM. Geometric parameters in nucleic acids: sugar and phosphate constituents. *J. Am. Chem. Soc.* 1996; 118:519–528.
- Golden BL, Kim H, Chase E. Crystal structure of a phage Twort group I ribozyme-product complex. *Nat. Struct. Mol. Biol.* 2004; 12:82–89. [PubMed: 15580277]
- Guo F, Gooding AR, Cech TR. Structure of the *Tetrahymena* ribozyme: Base triple sandwich and a metal ion at the active site. *Mol. Cell.* 2004; 16:351–32. [PubMed: 15525509]
- Kent WJ, Sugnet CW, Furey TS, Roskin KM, Pringle TH, Zahler AM, Haussler D. The human genome browser at UCSC. *Genome Res.* 2002; 12:996–1006. [PubMed: 12045153]
- Lipps HJ, Rhodes D. G-quadruplex structures: *in vivo* evidence and function. *Trends in Cell Biol.* 2009; 19:412–422.
- Monchard D, Teulade-Fichou MP. A hitchhiker's guide to G-quadruplex ligands. *Org. Biomol. Chem.* 2008; 6:627–636. [PubMed: 18264563]
- Neidle S. The structures of quadruplex nucleic acids and their drug complexes. *Curr. Opin. Struct. Biol.* 2009; 19:239–250. [PubMed: 19487118]

- Nielsen JT, Arar K, Petersen M. Solution structure of a locked nucleic acid modified quadruplex: Introducing the V4 folding topology. *Angew. Chem. Int. Edn.* 2009; 48:3009–3113.
- Nilges M, Habazettl J, Brünger AT, Holak TA. Relaxation matrix refinement of the solution structure of squash trypsin inhibitor. *J Mol Biol.* 1991; 21:499–510. [PubMed: 2051485]
- Ou T, Lu Y, Huang Z, Wong K, Gu L. G-quadruplexes: targets in anti-cancer drug design. *Chem. Med. Biochem.* 2008; 3:690–713.
- Parkinson GN, Lee MP, Neidle S. Crystal structure of parallel quadruplexes from human telomeric DNA. *Nature.* 2002; 417:876–880. [PubMed: 12050675]
- Patel DJ, Kozlowski SA, Nordheim A, Rich A. Right-handed and left-handed DNA: Studies of B-DNA and Z-DNA by using proton nuclear Overhauser effect and phosphorus NMR. *Proc. Natl. Acad. Scis. USA.* 1982; 79:1413–1417.
- Patel DJ, Phan AT, Kuryavyi V. Human telomere, oncogenic promotor and 5'-UTR G-quadruplexes: diverse higher order DNA and RNA targets for cancer therapeutics. *Nucleic Acids Res.* 2007; 35:7429–7455. [PubMed: 17913750]
- Phan AT. Long-range imino proton-<sup>13</sup>C J-couplings and the through-bond correlation of imino and non-exchangeable protons in unlabeled DNA. *J. Biomol. NMR.* 2000; 16:175–178. [PubMed: 10723997]
- Phan AT, Patel DJ. A site-specific low-enrichment <sup>15</sup>N, <sup>13</sup>C isotope-labeling approach to unambiguous NMR spectral assignments in nucleic acids. *J. Am. Chem. Soc.* 2002; 124:1160–1161. [PubMed: 11841271]
- Phan AT, Kuryavyi V, Patel DJ. DNA architecture from G to Z. *Curr. Opin. Struct. Biol.* 2006; 16:288–298. [PubMed: 16714104]
- Phan AT, Kuryavyi V, Burge S, Neidle S, Patel DJ. Structure of an unprecedented G-quadruplex scaffold in the human *c-kit* promotor. *J. Am. Chem. Soc.* 2007; 129:4386–4392. [PubMed: 17362008]
- Phan AT, Mody YS, Patel DJ. Propeller-type parallel-stranded G-quadruplexes in the human *c-myc* promoter. *J. Am. Chem. Soc.* 2004; 126:8710–8716. [PubMed: 15250723]
- Qin Y, Hurley LH. Structures, folding patterns and functions of intramolecular DNA G-quadruplexes found in eukaryotic promoter regions. *Biochimie.* 2008; 90:1149–1171. [PubMed: 18355457]
- Stahley MR, Strobel SA. Structural evidence for a two-metal-ion mechanism of Group I intron splicing. *Science.* 2005; 309:1587–1590. [PubMed: 16141079]
- Stahley MR, Strobel SA. RNA splicing: group I intron crystal structures reveal the basis of splice site selection and metal ion catalysis. *Curr. Opin. Struct. Biol.* 2006; 16:319–326. [PubMed: 16697179]
- Stein EG, Rice LM, Brünger AT. Torsion angle molecular dynamics: a new, efficient tool for NMR structure calculation. *J. Magn. Reson.* 1997; 124:154–164. [PubMed: 9424305]
- Wang Y, Patel DJ. Solution structure of the *Tetrahymena* d(T<sub>2</sub>G<sub>4</sub>)<sub>4</sub> G-tetraplex. *Structure.* 1994; 2:1141–1156. [PubMed: 7704525]
- Wu Y, Shin-ya K, Brosh RM. FANCI helicase defective in Fanconi Anemia and breast cancer unwinds G-quadruplex DNA to defend genomic stability. *Mol. Cell. Biol.* 2008; 28:4116–4128. [PubMed: 18426915]
- Wu Y, Suhasini AN, Brosh RM. Welcome to the family of FANCI-like helicases to the block of genome stability maintenance proteins. *Cell. Mol. Life Sci.* 2009; 66:1209–1222. [PubMed: 19099189]
- Zhang N, Gorin A, Majumdar A, Kettani A, Chernichenko N, Skripkin E, Patel DJ. V-shaped scaffold: A new architectural motif identified in an A•(G•G•G•G) pentad-containing dimeric DNA quadruplex involving stacked G(*syn*)•G(*anti*)•G(*anti*)•G(*anti*) tetrads. *J. Mol. Biol.* 2001; 311:1063–1079. [PubMed: 11531340]

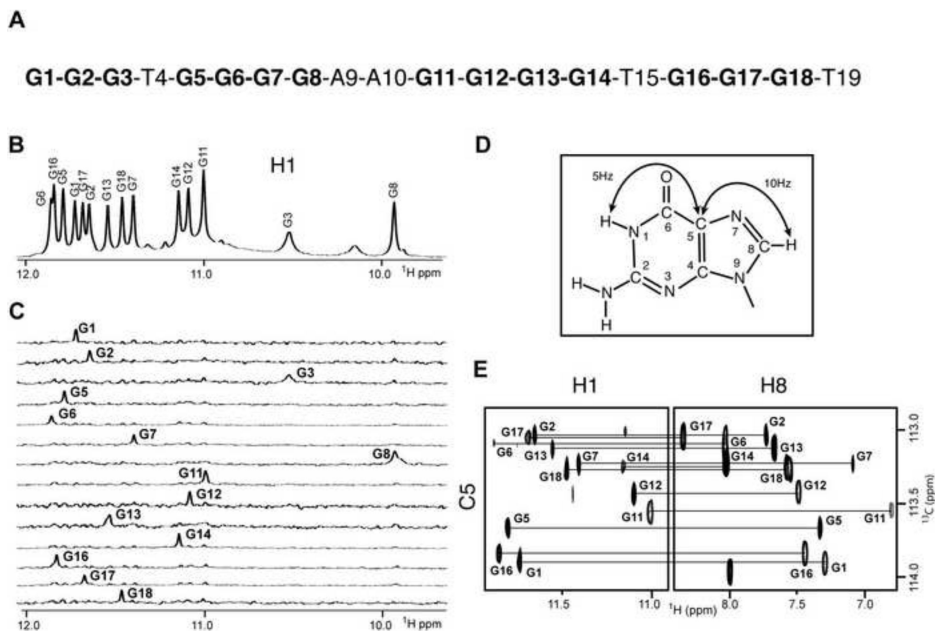


**Figure 1. NMR Spectra and Assignments of human *chII* Intronic 19-mer Sequence in 50 mM K<sup>+</sup>, 5 mM Phosphate-H<sub>2</sub>O Buffer, pH 6.8, at 25 °C**

(A) Sequence of the 19-mer human *chII* intronic DNA. (B) Imino proton NMR spectrum of *chII* sequence. Unambiguous guanosine imino proton assignments are listed over the spectrum. (C) Guanosine imino protons were assigned in <sup>15</sup>N-filtered NMR spectra of samples containing 2% uniformly-<sup>15</sup>N-labeled guanines at the indicated positions. (D) A schematic indicating long-range J couplings used to correlate imino and H8 protons within the guanosine base. (E) H8 proton assignments of *chII* intronic sequence by through-bond correlations between guanosine imino and H8 protons via <sup>13</sup>C5 at natural abundance, using long-range J couplings shown in (D).

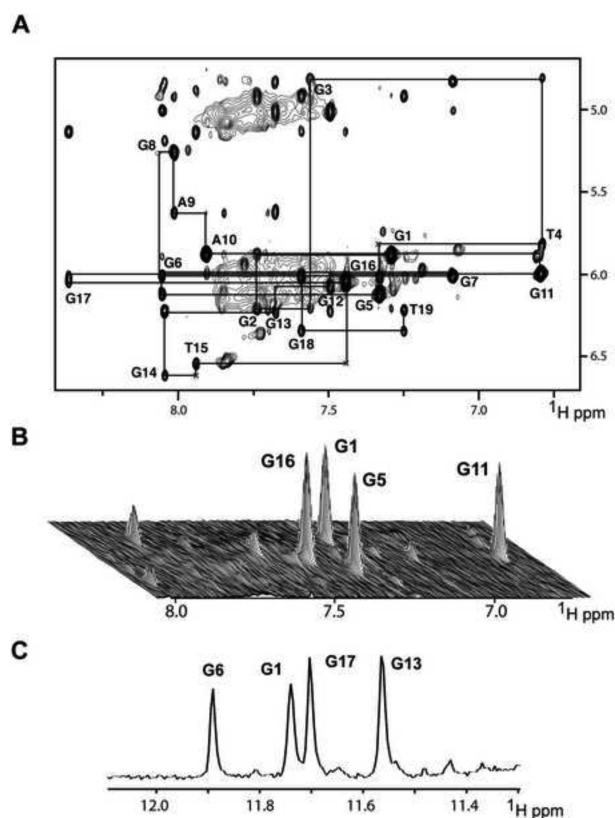


**Figure 2. Non-exchangeable Proton Assignments of *chII* Intronic 19-mer Sequence in 50 mM K<sup>+</sup>, 5 mM phosphate-<sup>2</sup>H<sub>2</sub>O buffer, pH 6.8, at 25°C**

(A) Expanded NOESY contour plot (200 ms mixing time) correlating base and sugar H1' protons. The line connectivities trace NOEs between a base proton (H8 or H6) and its own and 5'-flanking sugar H1' protons. Intraresidue base to sugar H1' NOEs are labeled with residue numbers. (B) Stacked plot of short mixing time (50 ms) NOESY data set under same buffer conditions as in (A). The strong intraresidue guanosine H8-H1' cross-peaks (*syn* glycosidic bonds) are labeled and can be distinguished from weak cross-peaks (*anti* glycosidic bonds). (C) Imino proton NMR spectrum of *chII* intronic sequence recorded after 45 min following transfer after lyophilization from H<sub>2</sub>O to <sup>2</sup>H<sub>2</sub>O solution. Assignments of slowly exchanging imino protons are listed over the spectrum.

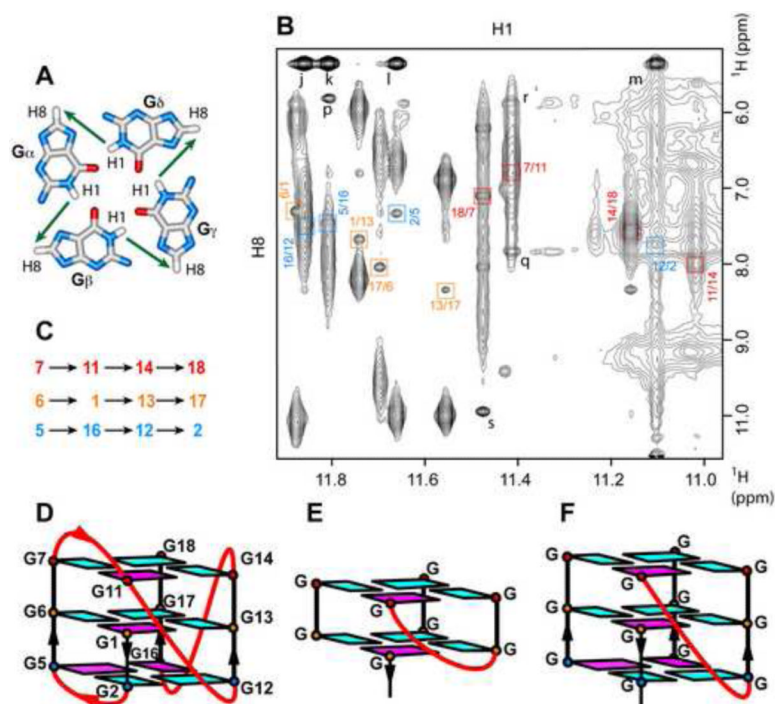


**Figure 3. Assignment of Individual G-tetrads within the *chll* G-Quadruplex**  
 (A) Characteristic guanosine imino-H8 NOE connectivity patterns around a  $G\alpha \cdot G\beta \cdot G\gamma \cdot G\delta$  tetrad as indicated by arrows. (B) Expanded contour plot showing imino to H8 connectivities of *chll* intronic 19-mer sequence in 50 mM  $K^+$ , 5 mM phosphate- $H_2O$  buffer, pH 6.8, at 25 °C. Cross-peaks identifying connectivities within individual G-tetrads are color-coded, with each cross-peak framed and labeled with the residue number of guanosine imino proton in the first position and that of the H8 proton in the second position. (C) Guanosine imino-H8 connectivities observed for G1•G13•G17•G6 (orange), G7•G11•G14•G18 (red) and G2•G5•G16•G12 (blue) G-tetrads. (D) Schematic representation of the *chll* intronic G-quadruplex fold. *Anti* bases are indicated in cyan, while *syn* bases are indicated in magenta. (E) Schematic of a V-shaped loop spanning two G-tetrad planes. (F) Schematic of a V-shaped loop spanning three G-tetrad planes.

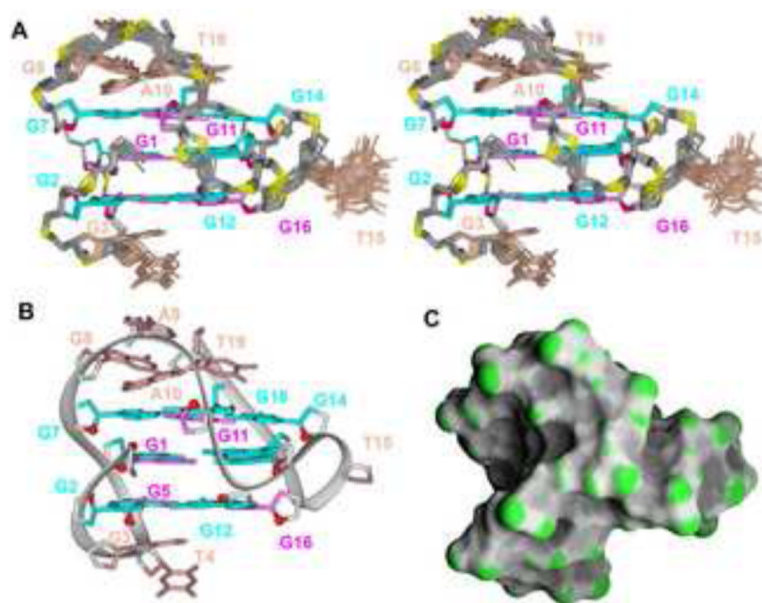


**Figure 4. Solution Structure of the *chII* G-Quadruplex in  $K^+$ -containing solution**  
 (A) Stereo view of 17 superpositioned refined structures. Guanine bases in the G-tetrad core are colored cyan (*anti*) or magenta (*syn*). Bases in connecting loops are in biscuit color, with the backbone in grey and phosphorus and oxygen atoms in yellow and red, respectively. (B) Ribbon and (C) surface representations of a representative refined structure.

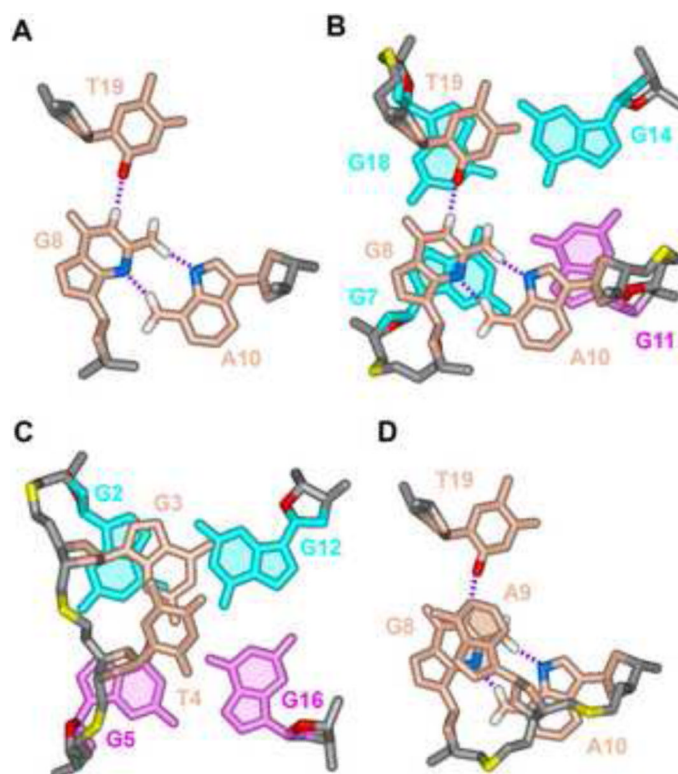


**Figure 5. Pairing and Stacking Alignments within the Loops Segments of the *chII* G-quadruplex in K<sup>+</sup>-containing Solution**

(A) Pairing alignment in the T19•G8•A10 triple. (B) Stacking between the T19•G8•A10 triple (biscuit) and the G7•G11•G14•G18 G-tetrad (cyan). (C) Stacking between the G3 base (biscuit) and the G2•G5•G16•G12 G-tetrad (cyan). (D) Stacking of A9 over the T19•G8•A10 triple.



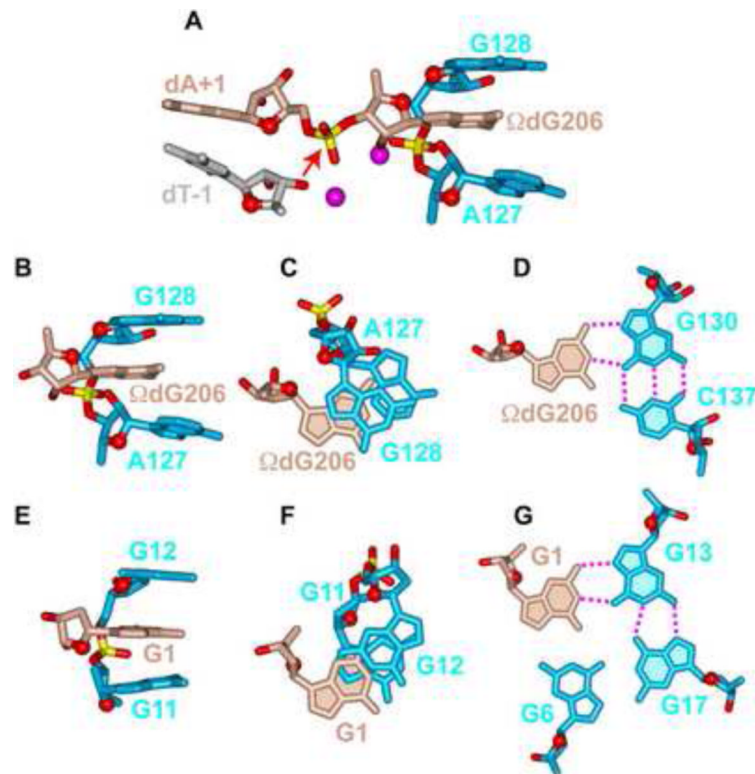


**Figure 6. Comparison of a Guanosine Intercalated Between the G-G step in *Azoarcus* Group I Intron and in the *chlI* intronic G-Quadruplex**

(A) The G-binding motif in the crystal structure of the *Azoarcus* Group I intron (Adams et al., 2004). Note that partial intercalation of  $\Omega$ dG206 between A127 and G128 assists in positioning the phosphate between  $\Omega$ dG206 and dA+1 for in-line attack by the 2'-OH of dT-1 (designated by a red arrow). The scissible phosphate is flanked by  $Mg^{2+}$  cations shown as magenta balls. Phosphorus and oxygen atoms are colored in yellow and red, respectively. (B) Side and (C) look-down views of the intercalation of  $\Omega$ dG206 between a G-G step and (D) hydrogen-bonding of Watson-Crick edge of  $\Omega$ dG206 with Hoogsteen edge of G130 in the crystal structure of the *Azoarcus* Group I intron (Adams et al., 2004). (E) Side and (F) look-down views of the intercalation of G1 between the G11-G12 step and (G) hydrogen-bonding of Watson-Crick edge of G1 with Hoogsteen edge of G13 in the NMR-based solution structure of the *chlI* intronic G-quadruplex reported in this study. (H) The postulated in line attack by a 3' -OH on the scissible phosphate is shown by an arrow. Phosphorus and oxygen atoms are colored in yellow and red, respectively.

**Table 1**Statistics of NMR restraints-guided computations of *chlI* intronic quadruplex.

<b>A. NMR restraints</b>		
<b>Distance restraints<sup>a</sup></b>	<b>Non-exchangeable</b>	<b>Exchangeable</b>
Intra-residue distance restraints	120	0
Sequential ( <i>i, i+1</i> ) distance restraints	55	5
Long-range ( <i>i, i+2</i> ) distance restraints	3	42
Other restraints		
Hydrogen bonding restraints (H-N, H-O, and heavy atoms)		52
Torsion angle restraints <sup>a</sup>		49
Intensity restraints		
Non-exchangeable protons (each of five mixing times)		178

<b>B. Structure statistics in 17 molecules following the intensity refinement</b>		
NOE violations		
Number (> 0.2Å)	0.0±0.0	
r.m.s.d. of violations	0.02±0.00	
Deviations from the ideal covalent geometry		
Bond lengths (Å)	0.01±0.00	
Bond angles (deg.)	0.83±0.01	
Impropers (deg)	0.30±0.01	
NMR R-factor (R <sub>1/6</sub> )	0.02±0.02	
Pairwise all heavy atom r.m.s.d. values (17 refined structures)		
All heavy atoms except T15	0.47±0.12	
All heavy atoms	0.64±0.15	

<sup>a</sup>The residues G1, G5, G11, G16 were restrained to  $\chi$  values in the 60 ( $\pm 30$ )° range, characteristic of *syn* glycosidic torsion angles, identified experimentally. All other residues were restrained to  $\chi$  values in the 240 ( $\pm 70$ )° range, characteristic of *anti* glycosidic torsion values. The  $\epsilon$  of the residues G1-G18 was restrained to the stereochemically allowed range 225 ( $\pm 75$ )°. The  $\gamma$  torsion angle of the residues 1, 2, 4, 7, 8, 9, 17, 18, 19 was restrained to the values of 60 ( $\pm 35$ )°, for residues 5, 10, 11 to 180 ( $\pm 35$ )°, identified experimentally.